

## Quantitative analysis of senile plaques in Alzheimer disease: Observation of log-normal size distribution and molecular epidemiology of differences associated with apolipoprotein E genotype and trisomy 21 (Down syndrome)

B. T. HYMAN\*, H. L. WEST\*, G. W. REBECK\*, S. V. BULDYREV†, R. N. MANTEGNA†, M. UKLEJA†, S. HAVLIN‡, AND H. E. STANLEY†

\*Neurology Service, Massachusetts General Hospital, Boston, MA 02114; †Center for Polymer Studies, Department of Physics, Boston University, Boston, MA 02215; and ‡Department of Physics, Bar-Ilan University, Ramat-Gan, Israel

Communicated by Charles R. Cantor, Boston University, Boston, MA, January 3, 1995

**ABSTRACT** The discovery that the  $\epsilon 4$  allele of the apolipoprotein E (apoE) gene is a putative risk factor for Alzheimer disease (AD) in the general population has highlighted the role of genetic influences in this extremely common and disabling illness. It has long been recognized that another genetic abnormality, trisomy 21 (Down syndrome), is associated with early and severe development of AD neuropathological lesions. It remains a challenge, however, to understand how these facts relate to the pathological changes in the brains of AD patients. We used computerized image analysis to examine the size distribution of one of the characteristic neuropathological lesions in AD, deposits of A $\beta$  peptide in senile plaques (SPs). Surprisingly, we find that a log-normal distribution fits the SP size distribution quite well, motivating a porous model of SP morphogenesis. We then analyzed SP size distribution curves in genotypically defined subgroups of AD patients. The data demonstrate that both apoE  $\epsilon 4$ /AD and trisomy 21/AD lead to increased amyloid deposition, but by apparently different mechanisms. The size distribution curve is shifted toward larger plaques in trisomy 21/AD, probably reflecting increased A $\beta$  production. In apoE  $\epsilon 4$ /AD, the size distribution is unchanged but the number of SP is increased compared to apoE  $\epsilon 3$ , suggesting increased probability of SP initiation. These results demonstrate that subgroups of AD patients defined on the basis of molecular characteristics have quantitatively different neuropathological phenotypes.

The recent revolution in the molecular biology of disease has led to the development of molecular epidemiology, in which a population of individuals with a disease is subdivided according to molecular characteristics. Although rare families with Alzheimer disease (AD) have been linked to mutations in the amyloid precursor protein (APP) on chromosome 21 (1) or to an unknown gene on chromosome 14 (2), by far the most common genetic predisposition for AD is conferred by inheritance of the  $\epsilon 4$  allele of the apolipoprotein E (apoE) gene ( $\epsilon 4$ , gene; E4, protein). The apoE  $\epsilon 4$  allele is overrepresented by  $\approx 4$ -fold in AD compared to age-matched control populations (3–5). Although the apoE  $\epsilon 4$  allele frequency in the general population is only 0.14 (6), it is present in  $>50\%$  of the patients with AD that present to AD clinics (3–5). Another genetic predisposition to AD is trisomy 21, in which essentially all individuals who live to their fifth or sixth decade develop severe neuropathological changes typical of AD (7). It is unknown how these genetic alterations are related to the fundamental pathological alterations of the disease, specifically the deposition of A $\beta$  amyloid peptide as senile plaques

(SPs). There is a need to define the phenotypic correlations of these subgroups to forge a link between molecular epidemiology and pathophysiology.

SPs consist primarily of fibrillar deposits of a 39- to 42-amino acid peptide, A $\beta$ , which is derived from the transmembrane domain and extracellular portion of APP. Normal metabolism of APP leads to multiple degradation fragments, including small amounts of soluble A $\beta$ , which is present in tissues, plasma, and cerebrospinal fluid (8, 9). A $\beta$  is partially hydrophobic and can self-aggregate into  $\beta$ -pleated sheets (10, 11). Although the exact relationship between deposition of A $\beta$  and dementia remains uncertain (12–14), clinical studies in trisomy 21/AD and in apoE  $\epsilon 4$ /AD show that there is increased deposition of A $\beta$  in both instances (4, 15, 16). We have now applied tools derived from the study of polymer formation (17) to study the morphogenesis of SPs, particularly with regard to possible genetic influences.

### METHODS

Tissue from 40 AD (age  $78.3 \pm 9.4$  years, mean  $\pm$  SD) and 7 elderly demented trisomy 21 (age  $60.8 \pm 4.2$  years) patients was studied. Tissue samples were obtained from the Massachusetts Alzheimer Disease Research Center brain bank. All patients had a clinical history of dementia confirmed to be AD by neuropathological examination of paraffin-embedded Bielschowski-stained sections according to the CERAD protocol (18). The tissue used in this study was 50- $\mu$ m sections of the temporal lobe that were immunostained with antibody 10D5 (19), a monoclonal antibody directed against A $\beta$ . A Bioquant image analysis system was used to semiautomatically assess SP number and cross-sectional area (13), from which the size distribution of plaques was calculated (Fig. 1).

In brief, immunostaining was carried out by using a horse-radish peroxidase-linked anti-mouse secondary antibody and diaminobenzidine as chromagen. Thus A $\beta$  deposits are dark brown against a blank background. A region 780  $\mu$ m wide by the depth of the cortex was examined in the inferior bank of the superior temporal sulcus,  $\approx 1$  cm from the crown of the gyrus. Consecutive  $\times 160$  magnification images from the pial surface to the gray/white junction were obtained by using a DAGE MTI CCD72 camera and digitized via a TARGA board. The Bioquant image analysis software allows identification of objects based on thresholding of the optical density and, thus, automatically will identify the dark A $\beta$  deposits. Operator editing was used to remove artifacts and vessel-associated A $\beta$  deposits and to separate touching structures (4, 13).

The publication costs of this article were defrayed in part by page charge payment. This article must therefore be hereby marked "advertisement" in accordance with 18 U.S.C. §1734 solely to indicate this fact.

Abbreviations: apoE, apolipoprotein E; AD, Alzheimer disease; SP, senile plaque; APP, amyloid precursor protein.

The superior temporal sulcus was chosen because it is consistently affected in AD and is characteristic of the degree of involvement of association cortices (20). Moreover, the superior temporal sulcus is a high-order association cortex and is one of only three trimodal association areas in the brain (21). As such, alterations here might be expected to impair the higher-order cognitive functions typically involved in AD-related dementia. Finally, the superior temporal sulcus region

is anatomically well defined allowing for matching of exact areas among patients. All morphological studies were performed without knowledge of clinical information or apoE genotype. ApoE genotypes were determined by using a PCR-based assay (4).

## RESULTS

**Development of Theory and Analysis of SP Size Distribution.** We have studied SP size distribution histograms  $P(V)$ , where  $P(V)\Delta V$  is the fraction of SPs with a volume in the range  $V$  to  $V + \Delta V$ . Consideration of analogous problems in statistical physics (22) and of the biological issues influencing SP growth until reaching a steady state (13) leads to the following three possible models for the rate of increase in volume  $V$  of SPs.

(i)  $dV/dt = k(t)$ , where  $k(t)$  is a parameter that changes with time in a random fashion around a positive average value until plaque size reaches a steady state. In this case, the histogram  $P(V)$ , giving the number of SPs of volume  $V$ , is a Gaussian.

(ii)  $dV/dt = k(t)S$ , where  $S$  is the external surface area. For spheres,  $S$  is proportional to  $r^2$ , while volume  $V$  is proportional to  $r^3$ ; here  $r$  denotes the typical radius. Hence, one can rewrite the equation in terms of  $r$  as  $dr/dt = k(t)$ . The solution of this equation produces a histogram that is Gaussian in the variable  $r$ .

(iii)  $dV/dt = k(t)V$ , i.e., the rate is proportional to the volume. In this case, the histogram  $P(V)$  is dramatically skewed to the right. However, if we change variables from  $V$  to  $x = \log V$ , then  $dx/dt = k(t)$ ; the distribution is Gaussian in this new variable and is thus log-normal (22, 23).

The distribution of the cross-sectional area  $A$ ,  $P(A)$ , rather than  $P(V)$  is plotted because  $A$  was directly measured. In accord with previous observations, we found that the profile of plaque sizes when plotted as a function of  $A$  along a linear axis is far from being Gaussian but instead is skewed to the right (13, 24, 25) (Fig. 2a). We have now found that the SP size distribution profile can be approximated by a log-normal distribution. Indeed, when the distribution is plotted as a function of  $\log A$ , it has the shape of a Gaussian (Fig. 2b). Note that for roughly spherical objects, a log-normal distribution of cross-sections yields a similar distribution as the volumes. Thus our data support models that result in a log-normal distribution and are inconsistent with models that predict a Gaussian distribution.

In general, a Gaussian for the  $P(V)$  histogram is usually found when  $V$  is proportional to the sum of several parameters, each of which has independent fluctuations about its mean. In contrast, a log-normal distribution for the histogram occurs when  $V$  is proportional to the product of several parameters (23, 26, 27), each of which has independent fluctuations about its mean. We have considered alternative explanations of the log-normal size distribution. If, for example, the coefficient  $k(t)$  is proportional to the product of random variables, each with independent fluctuations about the mean, then the SP size distribution would also be log-normal. Indeed, if  $k(t)$  were different for different lamina and the SP size distribution from

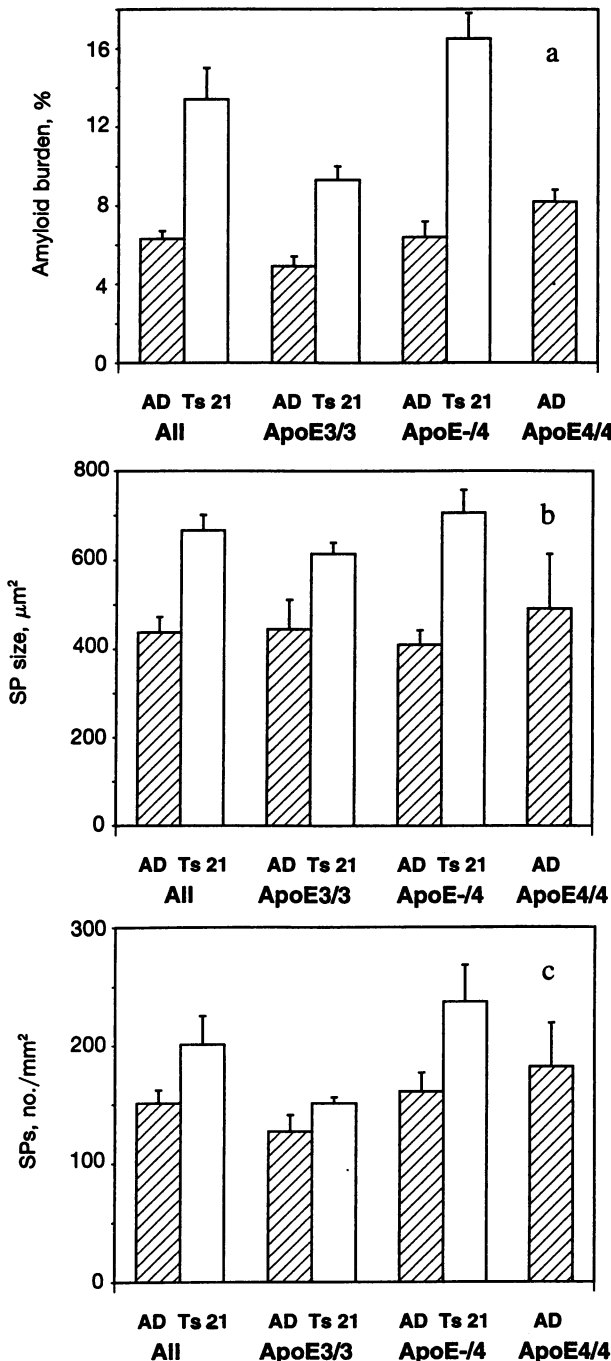


FIG. 1. Comparison of amyloid burden, SP size, and SP number per unit area in AD and trisomy 21 (Ts 21): Effect of apoE genotype. Amyloid burden (percent of cortex covered by  $A\beta$ , excluding vessel-associated immunostaining) (a), cross-sectional area (SP size) (b), and SP number per unit area (c) are shown as mean  $\pm$  SEM. The left-most columns contain data from all AD ( $n = 40$ ) and trisomy 21/AD ( $n = 7$ ) samples. Comparison of AD (hatched bars) and trisomy 21/AD (open bars) reveals statistically significant differences in SP size ( $P < 0.001$ ) and amyloid burden ( $P < 0.001$ ), but not SP number. The right portions of the graphs show the data separated by apoE genotype.

Genotype was determined by a PCR-based assay of the apoE gene (4). Thirty-seven of the original 40 samples were apoE  $\epsilon 3/3$  ( $n = 15$ ), apoE  $\epsilon 3/4$  ( $n = 15$ ), or apoE  $\epsilon 4/4$  ( $n = 7$ ). There are significant differences in amyloid deposition among genotypes. Analysis of variance with post hoc Fisher protected least significant difference showed significant ( $P < 0.05$ ) differences (i) between apoE  $\epsilon 3/3$  and apoE  $\epsilon 4/4$  for amyloid burden, (ii) between apoE  $\epsilon 3/3$  and apoE  $\epsilon 4/4$  and between apoE  $\epsilon 3/4$  and apoE  $\epsilon 4/4$  for SP number, and (iii) no difference in SP size. Similar differences in SP number but not size are seen among groups in trisomy 21/AD that have either zero ( $n = 3$ ) or one apoE  $\epsilon 4$  allele ( $n = 4$ ; 3 individuals with apoE  $\epsilon 3/4$  and 1 with apoE  $\epsilon 2/4$ ) ( $P < 0.05$ ) (for detailed description of these samples, see ref. 15).

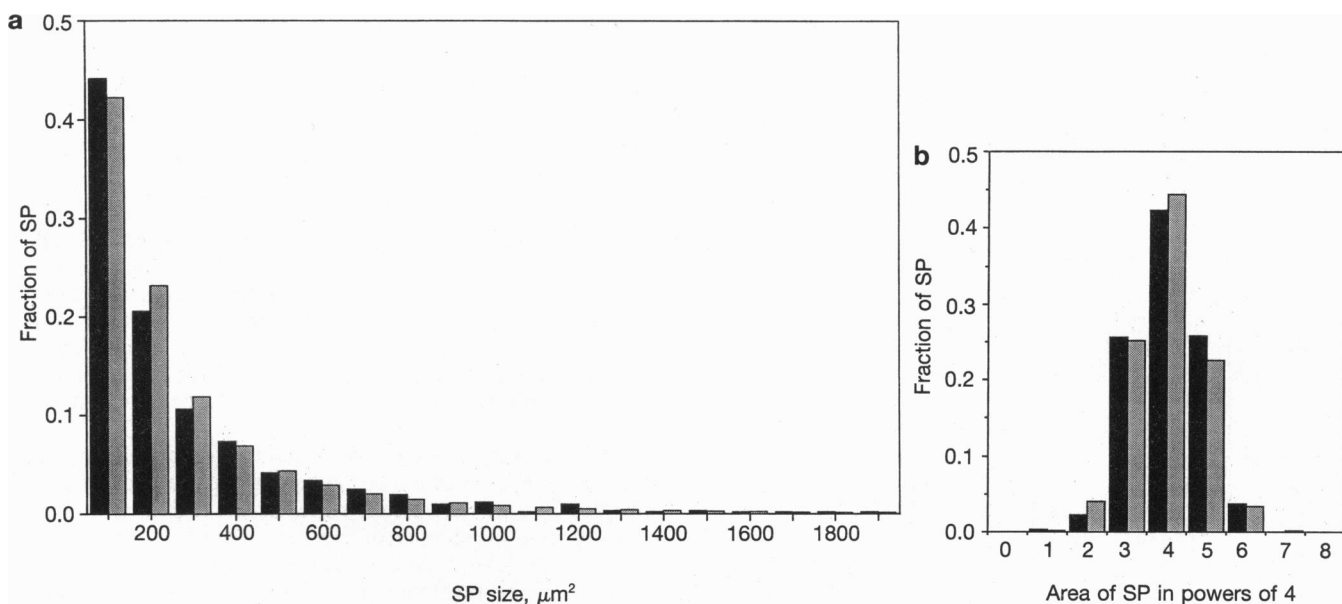


FIG. 2. SP size profile distribution histograms of an AD patient. A 50- $\mu\text{m}$ -thick section of the temporal lobe was immunostained with anti-A $\beta$  monoclonal antibody 10D5. Four adjacent regions, each 780  $\mu\text{m}$  wide by the depth of the cortex, in the inferior bank of the superior temporal sulcus located  $\approx$ 1 cm from the crest of the middle temporal gyrus were analyzed. This area contained 917 SPs. Video images (DAGE-MTI CCD72) were captured by using a Grafica 486/33 computer running Bioquant image analysis software. After manual editing to remove artifacts and vessel-associated staining, the software outlined each SP, and the number of plaques and size of each plaque were recorded. The histogram of plaque size (solid bars) is plotted in bins of 100  $\mu\text{m}^2$  on a linear scale (a) or in bins of powers of 4 on a logarithmic base-4 scale (b). A curve generated from a theoretical log-normal distribution with the same mean and variance is shown as shaded bars to illustrate how well this distribution fits the data.

each lamina were Gaussian, then the overall distribution for all lamina could be log-normal. To rule out this possibility, we computed the distributions of plaques within an observation window of size 500  $\times$  500  $\mu\text{m}$  that we slide inside broad samples of a cortical traverse section of 3500  $\mu\text{m}$  long and  $\approx$ 3000  $\mu\text{m}$  deep. For each position of the window, we measured the number of plaques within the window and the mean and standard deviation of the log-normal distributions. This method allows us to obtain 11 parallel profiles of the studied quantities. Each profile has 50 data points that correspond to different depths of cortex from 0 depth on the cortical surface to the maximal depth at the gray-white boundary. The distance between successive profiles is 300  $\mu\text{m}$ . We found that the profiles are similar at all depths. These similarities suggest the presence of strips with a high density of plaques that are parallel to the cortical surface, e.g., in the laminae. The parameters of the log-normal distribution do not change systematically along the profiles, staying almost constant for all the positions of the observation window. This indicates that the process of plaque growth does not change for different cortical depths.

**Influence of ApoE Genotype and Trisomy 21 on Amyloid Deposition.** The observation that SP size is similar for all cases studied and fits the log-normal law allows quantitative comparison across different subgroups of AD patients defined by molecular characteristics. This is of particular relevance in two instances where increased amyloid deposition occurs, apoE  $\epsilon$ 4/AD and trisomy 21 AD. Jarrett and Lansbury (28) hypothesize that SP formation involves two major steps: a nucleation phenomenon in which a relatively small number of A $\beta$  molecules aggregate to reach a threshold size of a stable nidus, followed by a growth/dissolution phase in which SP enlarge until reaching steady state. This formulation suggests two ways in which there could be increased amyloid deposition, by increased successful nidus formation and/or increased rate of growth. If there were increased availability of A $\beta$ , we predict that the SP size distribution curve would shift to the right as SP became, on average, larger. On the other hand, increased

formation or stability of individual nucleation sites would lead to the same size distribution but increased numbers of SPs.

We tested the first prediction by studying elderly trisomy 21 individuals with AD, where there is elevated deposition of A $\beta$  presumably due to the triplication and overproduction of APP. Comparison of >3000 SPs from 7 elderly demented trisomy 21/AD patients to >19,000 SPs from 40 AD patients showed increased amyloid deposition in trisomy 21/AD ( $P < 0.001$ ) (Fig. 1b). The trisomy 21/AD curve is shifted to the right toward larger size ( $P < 0.001$ ) (Fig. 3). Note that the x axis is a logarithmic base-4 scale, so that a move to the right of 1 unit is a 4-fold increase. These results provide quantitative evidence consistent with the idea that increased A $\beta$  production is the cause of the increased amyloid deposition in trisomy 21. A potentially confounding issue is the fact that the trisomy 21/AD individuals are younger than the nontrisomy 21 AD individuals. We asked whether age *per se* correlated with any of the quantitative measures of A $\beta$  deposition within the AD group, whose ages ranged from 62 to 95 years, or within the trisomy 21 individuals whose ages ranged from 57 to 67 years. No significant correlations were found, and in each case, the correlation coefficient was  $<0.20$  (not significant), suggesting no relationship between age and size or number of SPs or amyloid burden.

Inheritance of the apoE  $\epsilon$ 4 allele is also associated with increased deposition of A $\beta$  (Fig. 1c) (16). Because apoE binds hydrophobic macromolecules such as low density lipoproteins and transports them to specific receptors for cellular uptake, it has been suggested that one role of apoE in the pathophysiology of AD is to act as a clearance mechanism for A $\beta$  or A $\beta$  aggregates (4). This hypothesis is supported by the observations that apoE binds A $\beta$  *in vitro* (29, 30), and apoE (4, 31) and an apoE receptor protein, the low density lipoprotein receptor-related protein, are associated with SPs (4).

If apoE4 is less efficient than apoE3 at clearing soluble monomeric A $\beta$ , this would lead to a higher A $\beta$  level and, hence, to larger (and possibly more) deposits in individuals who inherit apoE  $\epsilon$ 4. Alternatively, if apoE4 is less efficient at

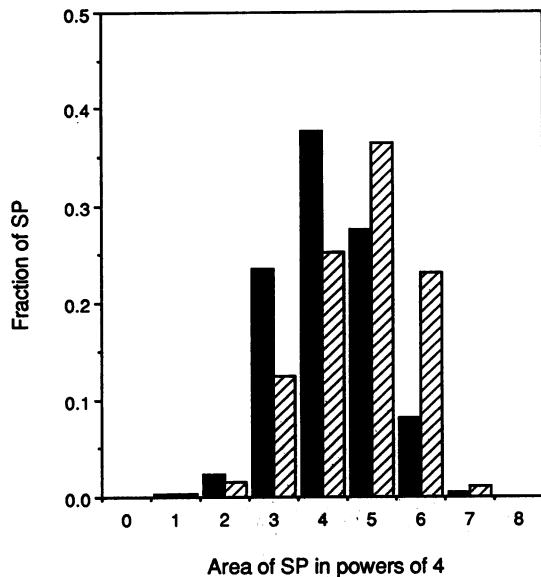


FIG. 3. Comparison of size distribution of SPs in AD and trisomy 21. The histogram of SP size distribution is plotted in bins of powers of 4 on a logarithmic base-4 scale. The histogram compares the data from measurements of >19,000 SPs from 40 AD patients (solid bars) to the distribution derived from examination of >3000 SPs in 7 elderly individuals with trisomy 21/AD (hatched bars) (four measurements in superior temporal sulcus and three measurements in inferior temporal cortex). Both distributions closely approximate a Gaussian distribution and, hence, are log-normal. The shapes of the AD and trisomy 21/AD distributions are essentially identical, but the trisomy 21/AD distribution is significantly shifted to the right ( $P < 0.001$ ).

clearing small A $\beta$  aggregates than apoE3, this would lead to an increased chance that an aggregate would reach a critical threshold size and lead to an increased SP number but not affect the size distribution. To test these two possibilities, we analyzed the size distribution data with the AD sample divided by apoE genotype. We found that the apoE  $\epsilon$ 4 genotype is associated with increased numbers of SPs (Fig. 1c). Different apoE genotypes have essentially identical size distribution profiles (Fig. 4). This result suggests that the likelihood of

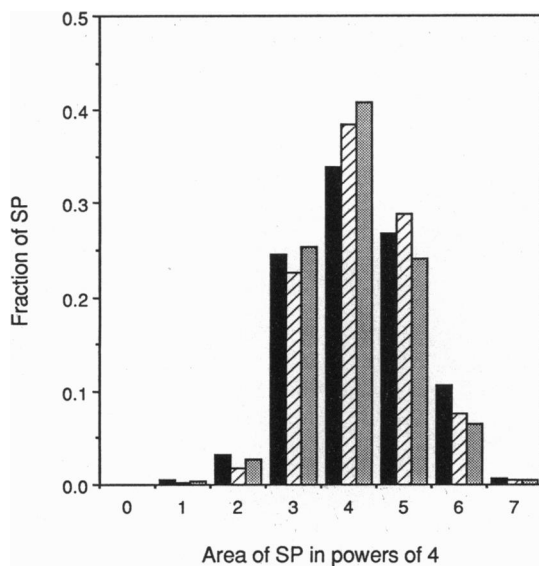


FIG. 4. SP size distribution of AD patients of defined ApoE genotype. Comparison of the SP size distributions of AD individuals who are apoE  $\epsilon$ 3/3 (shaded bars), apoE  $\epsilon$ 3/4 (hatched bars), or apoE  $\epsilon$ 4/4 (solid bars) reveals nearly identical size and shape profiles among the different genotypes. Samples are as described in Fig. 1.

successful nidus formation is greater with apoE. We postulate that either apoE4 (compare to apoE3) enhances precipitation of A $\beta$  as a pathological chaperone (31) or apoE normally has a role in clearing small aggregates and it is this function that is differentially performed by apoE3 or apoE4.

Subdividing the seven trisomy 21/AD samples according to apoE genotype reveals differences between genotypes even in this small group (Fig. 1). Individuals who had both trisomy 21 and had inherited apoE  $\epsilon$ 4 show a 2-fold higher amyloid burden than similarly aged trisomy 21 individuals who did not inherit an apoE  $\epsilon$ 4. Thus the combination of trisomy 21 (perhaps with increased amount of A $\beta$ ) and ApoE  $\epsilon$ 4 (perhaps with decreased clearance of A $\beta$  or A $\beta$  aggregates) leads to markedly elevated A $\beta$  deposition.

## DISCUSSION

These data lead to two major conclusions. (i) The analysis of SP size distribution motivates a mathematical model and provides a quantitative basis to support several conclusions regarding SP formation. The size distribution curve of SP is log-normal. This is a somewhat unusual property that is associated with certain physical systems. For example, a log-normal size distribution profile of SPs could result from a physical model in which the SP growth rate is proportional to the volume; this implies that the "surface" is not a compact surface. Instead a certain fraction of interior points is accessible to and in equilibrium with the neuropil, suggesting a porous rather than a compact structure for the plaque. Sponge-like or porous structures have been shown to be the case in a bicontinuous microemulsion that consists of an amphipathic film (a surfactant monolayer) separating a hydrophobic aggregate from the hydrophilic environment (32, 33). The interpretation that SPs are porous would also explain the puzzling observation that cut surfaces (rather than just the rim) of SPs immunostain for multiple SP-associated antigens, including apoE (4).

(ii) Our data demonstrate that subgroups of AD patients defined by molecular properties differ with regard to quantitative characteristics of a fundamental aspect of the pathology of the disease: deposition of A $\beta$ . Increased amyloid burden occurs in AD associated with both trisomy 21 and apoE  $\epsilon$ 4, implying an increased rate of A $\beta$  deposition in both circumstances. The results provide quantitative evidence that increased A $\beta$  levels underlie deposition in trisomy 21. By analogy, the same may hold true for patients who inherit the Swedish APP mutation, which leads to overproduction of A $\beta$  (34, 35). The current results also suggest that the association of apoE  $\epsilon$ 4 with increased A $\beta$  deposition may be due to increased initiation of SPs, perhaps related to increased stability or decreased clearance of A $\beta$  aggregates. Thus individuals who inherit both trisomy 21 and apoE  $\epsilon$ 4 develop extraordinarily high amyloid burdens (15). These observations fit with a formulation that the rate of A $\beta$  deposition is a reflection of the relative rates of A $\beta$  synthesis, aggregation, and clearance. Recent evidence suggesting that APP717 mutations lead to the production of a greater percentage of A $\beta$ (1-42), which has a greater tendency than A $\beta$ (1-40) to aggregate (36), also fits with this formulation. Thus, these data provide evidence favoring heterogeneity in the mechanisms of A $\beta$  deposition in different molecularly defined subgroups of AD patients.

We thank R. Tanzi, J. Penney, M. F. Beal, and J. Growdon for their thoughtful comments, and L. Cruz, D. Futer, A. L. Goldberger, P. Ivanov, L. Lipsitz, and F. Sciortino for contributions at the initial stages of this research. This research was supported by National Institutes of Health Grants AG08487 and PO50AG05134, and an award from the Metropolitan Life Foundation (B.T.H.). We thank the Massachusetts Alzheimer Disease Research Center Brain Bank (Dr.

E. T. Hedley-Whyte, director) for neuropathological diagnoses and access to tissue. H.L.W. is a Howard Hughes Medical Student Fellow.

1. Goate, A., Chartier-Harlin, M.-C. & Mullan, M. (1991) *Nature (London)* **349**, 704–707.
2. Schellenberg, G., Bird, T. D., Wijsman, E. M., Orr, H. T., Anderson, L., Nemens, E., White, J. A., Bonnycastle, L., Weber, J. L., Alonso, M. E., Potter, H., Heston, L. L. & Martin, G. M. (1992) *Science* **258**, 668–671.
3. Saunders, A. M., Strittmatter, W. J., Schmechel, D., St. George-Hyslop, P. H., Pericak-Vance, M. A., Joo, S. H., Rosi, B. L., Gusella, J. F., Crapper-MacLachlan, D. R., Alberts, M. J., Hulette, C., Crain, B., Goldgaber, D. & Roses, A. D. (1993) *Neurology* **43**, 1467–1472.
4. Rebeck, G. W., Reiter, J. S., Strickland, D. K. & Hyman, B. T. (1993) *Neuron* **11**, 575–580.
5. Poirier, J., Davignon, J., Bouthillier, D., Kogan, S., Bertrand, P. & Gauthier, S. (1993) *Lancet* **342**, 697–699.
6. Ordovas, J. M., Litwack-Klein, L., Wilson, P. W. F., Schaefer, M. M. & Schaefer, E. J. (1987) *J. Lipid Res.* **28**, 371–380.
7. Mann, D. M. A. (1988) *Mech. Ageing Dev.* **443**, 99–136.
8. Shoji, M., Golde, T. E., Ghiso, J., Cheung, T. T., Estus, S., Shaffer, L. M., Cai, X.-D., McKay, D. M., Tintner, R., Frangione, B. & Younkin, S. G. (1992) *Science* **258**, 126–129.
9. Seubert, P., Vigo-Pelfrey, C., Esch, F., Lee, M., Dovey, H., Davis, D., Sinha, S., Schlossmacher, M., Whaley, J., Swindlehurst, C., McCormack, R., Wolfert, R., Selkoe, D., Lieberburg, I. & Schenk, D. (1992) *Nature (London)* **359**, 325–327.
10. Jarrett, J. T. & Lansbury, P. T. (1993) *Cell* **73**, 1055–1058.
11. Burdick, D., Soreghan, B., Kwon, M., Kosmoski, J., Knauer, M., Henschen, A., Yates, J., Cotman, C. & Glabe, C. (1991) *J. Biol. Chem.* **267**, 546–554.
12. Arriagada, P. V., Growdon, J. H., Hedley-Whyte, E. T. & Hyman, B. T. (1992) *Neurology* **42**, 631–639.
13. Hyman, B. T., Marzloff, K. & Arriagada, P. V. (1993) *J. Neuro-pathol. Exp. Neurol.* **52**, 594–600.
14. Hyman, B. T. & Tanzi, R. E. (1992) *Curr. Opin. Neurol. Neurosurg.* **5**, 88–93.
15. Hyman, B. T., West, H. L., Rebeck, G. W., Lai, F. & Mann, D. M. A. (1995) *Arch. Neurol.*, in press.
16. Schmechel, D. E., Saunders, A. M., Strittmatter, W. J., Crain, B., Hulette, C., Joo, S. H., Pericak-Vance, M. A., Goldgaber, D. & Roses, A. D. (1993) *Proc. Natl. Acad. Sci. USA* **90**, 9649–9653.
17. Stanley, H. E. (1971) *Introduction to Phase Transitions and Critical Phenomena* (Oxford Univ. Press, London), pp. 1–121.
18. Mirra, S. S., Heyman, A. & McKeel, D. (1991) *Neurology* **41**, 479–486.
19. Hyman, B. T., Tanzi, R. E., Marzloff, K. M., Barbour, R. & Schenk, D. (1992) *J. Neuropathol. Exp. Neurol.* **51**, 76–83.
20. Arnold, S. E., Hyman, B. T., Flory, J., Damasio, A. R. & Van Hoesen, G. W. (1991) *Cerebral Cortex* **1**, 103–116.
21. Yeterian, E. & Pandya, D. (1989) in *Cerebral Cortex*, eds. Jones, E. G. & Peters, A. (Plenum, New York), pp. 1–53.
22. Granqvist, C. G. & Buhman, R. A. (1976) *J. Appl. Phys.* **47**, 2219–2200.
23. Montroll, E. W. & Shlesinger, M. F. (1982) *Proc. Natl. Acad. Sci. USA* **79**, 3380–3383.
24. Kawai, M., Cras, P. & Perry, G. (1992) *Brain Res.* **592**, 278–282.
25. Armstrong, R. A., Myers, D. & Smith, C. U. (1991) *Neurosci. Lett.* **127**, 223–226.
26. Pielou, E. C. (1969) *An Introduction to Mathematical Ecology* (Wiley-Interscience, New York).
27. Redner, S. (1990) *Am. J. Phys.* **58**, 267–273.
28. Jarrett, J. T. & Lansbury, P. T. (1992) *Biochemistry* **31**, 12345–12352.
29. Strittmatter, W. J., Weisgraber, K. H., Huang, D., Dong, L. M., Salvesen, G. S., Pericak-Vance, M., Schmechel, D., Saunders, A. M., Goldgaber, D. & Roses, A. D. (1993) *Proc. Natl. Acad. Sci. USA* **90**, 8098–8102.
30. Wisniewski, T., Golabek, A., Matsubara, E., Ghiso, J. & Frangione, B. (1993) *Biochem. Biophys. Res. Commun.* **192**, 359–365.
31. Wisniewski, T. & Frangione, B. (1992) *Neurosci. Lett.* **135**, 235–238.
32. Safran, S. A. (1994) *Statistical Thermodynamics of Surfaces, Interfaces, and Membranes* (Addison-Wesley, Reading, MA).
33. Grosberg, A. Y. & Khokhlov, A. R. (1994) *Statistical Physics of Macromolecules* (Am. Inst. of Physics, New York).
34. Cai, X.-D., Golde, T. E. & Younkin, S. G. (1993) *Science* **259**, 514–516.
35. Citron, M., Oltersdorf, T., Haass, C., McConlogue, L., Hung, A. Y., Seubert, P., Vigo-Pelfrey, C., Lieberburg, I. & Selkoe, D. J. (1992) *Nature (London)* **360**, 672–674.
36. Suzuki, N., Cheung, T. T., Cai, X.-D., Odaka, A., Otvos, L., Jr., Eckman, C., Golde, T. E. & Younkin, S. G. (1994) *Science* **264**, 1336–1340.